2021 43rd Annual International Conference of the
IEEE Engineering in Medicine & Biology Society (EMBC)
Oct 31 - Nov 4, 2021. Virtual Conference

Fast Prediction of RF-induced Heating for Sacral Neuromodulation System Exposed to Multi-Channel 2 RF Field at 3T MRI

Qianlong Lan, Ran Guo, Jiajun Chang, Jianfeng Zheng, *Member, IEEE*, Kyle Yu, and Ji Chen, *Senior Member, IEEE*

***Abstract*—This paper presents a fast method to predict the radiofrequency (RF) induced heating for Sacral Neuromodulation System (SNM) under multi-channel 2 (MC-2) RF field of 3 Tesla (T) magnetic resonance imaging (MRI) system by using the artificial neural network (ANN). The raw computational model for the SNM was based on the transfer function approach. The MC-2 parallel transmission RF field at 3T MRI exposure was considered for 2 independent channels, which have an exposure space of -15 dB to 15 dB magnitude difference and -180 degrees to 170 degrees phase difference. A total number of 535,680 study cases that cover all possible shimming conditions and the corresponding temperature rises are collected from raw calculation data. The ANN was used as the surrogate model to predict the temperature rises against the incident electromagnetic field distributions. 40320 cases were used for training while the rest data sets were used for testing. The ANN can estimate the temperature rises for each human model in a small exposure sampling space. The testing performance of the ANN has a correlation coefficient higher than 0.99 and the mean absolute error was less than $0.12^{\circ}C$. It is demonstrated that the ANN can be used as an efficient tool for quick temperature rise estimation under MRI 3T shimming.**

***Clinical Relevance*— The proposed ANN can be used to fast predict and alleviate the computation and simulation burden of the RF-induced heating for active implantable medical devices (AIMDs) under a 3T MRI environment based on the transfer function approach. It can also facilitate physicians with patient specific evaluation of RF-induced heating for AIMDs under MRI procedure.**

I. Introduction

The sacral neuromodulation (SNM) system is an active implantable medical device (AIMD) to treat the symptoms of overactive bladder, fecal incontinence, and urinary retention in patients who have failed or could not tolerate conservative treatments. However, due to the coupling with the radiofrequency (RF) field, RF-induced heating is a major safety concern when these patients need an MRI scan.

To estimate the RF-induced heating for SNM devices, the most common approach is to follow the method described as the Tier 3 Method in ISO/TS 10974 [1]. This method combines the incident electric field and the validated device model of the SNM system (also known as the transfer function) to estimate the RF-induced heating along with all clinically relevant pathways at different imaging landmarks in different human bodies. The transfer function model can be determined through the reciprocity approach while the electric field distributions inside the human body are obtained via rigorous numerical simulations in [2-3]. Per ISO/TS 10974, the in-vivo power deposition around the implant shall be determined for patients with different body shapes, at different imaging positions in MRI bore, and along all possible clinical trajectories. To achieve a comprehensive and conservative result for RF safety labeling, all these parameters must be completely studied and analyzed [4-7]. For high fields MRI systems, such as 3T MRI, additional factor such as RF shimming strategy also needs to be included in the study since the input power and phase from two excitation ports can be adjusted based on specific needs such as the B1+ field homogeneity [8]. However, the RF shimming needs to be evaluated for all patient body types, at all imaging positions, and along all possible implantable trajectories. This would require additional computational resources by a factor over 1000.

Preliminary studies have already shown that an artificial neural network (ANN) was one feasible solution to provide an efficient prediction of the MRI RF-induced heating for passive implantable medical devices (PIMDs) [9-11]. The network can work as a surrogate model to map the non-linear relationship between the parameters of PIMDs and the RF-induced heating. Similarly, for the SNM, it may also model the non-linear relationship between all possible shimming conditions and RF-induced heating, based on the transfer functions.

Ji Chen is with the ECE department at University of Houston, Houston, TX 80305 USA (corresponding author to provide phone: 713-743-4423; fax: 713-743-4444; e-mail: jchen18@uh.edu).

Qianlong Lan, Ran Guo, Jiajun Chang, and Jianfeng Zheng were with University of Houston, Houston, TX 77005 USA. (e-mail:qlan2@uh.edu; guoran188@gmail.com; jason.zhjf@gmail.com).

Kyle Yu was with William P. Clements High School, Sugar Land, TX 77479 USA. (e-mail:kyle.yu27@gmail.com)

In this paper, the MRI RF-induced heating for SNM devices under the exposure of a 3T MR RF coil is predicted. A total number of 535,680 study cases with incident electromagnetic field excitation magnitude interval of 1 dB and phase interval of 10 degrees that cover all possible shimming conditions and the corresponding temperature rises are collected from raw calculation data. Then, a part of the data (40,320 cases ≈ 7%) with incident electromagnetic field excitation magnitude interval of 5 dB and phase interval of 30 degrees was selected and used as a training set of the ANN, while the rest is used to test the performance of the ANN. Once this ANN has been tested or validated, the RF-induced heating can be estimated for all exposure conditions.

II. Methodology

A. In-vivo Simulation for Incident Electric Fields

Generally, an SNM device would have its lead inserted into the sacral foramen with electrodes positioned near the sacral nerve and the implantable pulse generator (IPG) placed in the buttock region. Five anatomically correct human models (Billie, Duke, Ella, Fats1, Fats2) from the Virtual Family project were used in the study [12,13]. Based on clinical recommendations, the lead tip electrodes should be placed at 3 target levels (S2, S3, S4) on each side (left, right) of the sacral nerve. The IPG can be located at two different positions within the buttock region at the either left or right body side. These trajectories all have a length of 300 mm and are developed based on clinical scenarios. In total, there are 24 different lead trajectories for each human body model as shown in Figure 1. The human body model is placed at the isocenter of the RF coil along the principal z-axis.

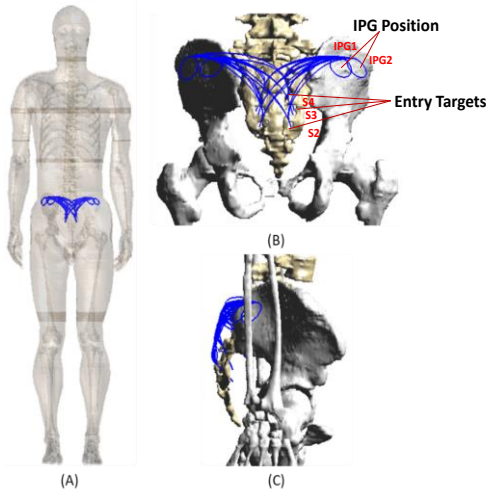

Figure 1. Trajectories for the adult male model (A); The IPG positions and entry targets of the SNM (B); Side view of the trajectories (C).

The numerical electromagnetic (EM) simulations were conducted using the SEMCAD X package (V14.4 Aletsch, SPEAG, Zurich, Switzerland) to obtain the tangential electric field. The Virtual Population models are used in the numerical simulations [14]. The computational RF coil model is a typical 16-rung 3T high-pass birdcage coil (diameter 750 mm and length 450 mm) with two channels (I channel and Q channel) at a frequency of 128 MHz. Considering the RF shimming effect at 3T, the MC-2 parallel transmission RF field was studied. The Q channel in this study was set with a magnitude of 0 dB and a phase of 0 degrees. I channel has a relative magnitude range from -15 dB to 15 dB with an interval of 1dB, and a relative phase range from -180 degrees to 170 degrees with an interval of 10 degrees. Thus, the total number of excitations would be $31 \times 36 = 1116$. The spatial resolution of the anatomical model uses a non-regular size that ranges between 0.5 to 2 mm for different regions and the resolution of the numerical grid size were set to 2 mm. The whole-body Specific Absorption Rate (SAR) and head SAR are limited to 2 W/kg and 3.2 W/kg for the normal operating mode. The uniaxial perfectly matched layers absorption boundary condition was used to truncate the computational region to mimic the real scanning conditions.

The tangential electric field of all these different configurations (trajectories, pathways, human models, excitations, and implantation positions, etc.) which contains 535,680 cases were obtained after the numerical simulation. Finally, the temperature rise can be calculated from the tangential electric field using the transfer function. All these simulation results will be defined as the raw data used for the study.

B. ANN

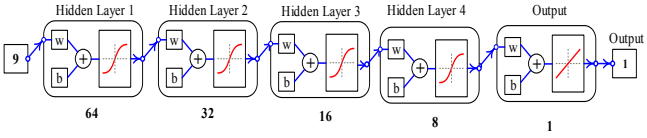

Figure 2. ANN architecture for the RF-induced heating prediction.

TABLE 1. ALL STUDY CONFIGURATIONS ARE USED AS THE RAW DATA.

Parameters	**Data**		
	Value	***Interval***	***Number of Values***
Human Model	Billie, Duke, Ella, Fats1, Fats2	NA	5
Electrode	E0, E3	NA	2
Medium Conductivity	0.47 S/m, 0.34 S/m	NA	2
Target Side	Left, Right	NA	2
Target Level	S2, S3, S4	NA	3
IPG Side	Left, Right	NA	2
IPG Position	IPG1, IPG2	NA	2
Excitation Magnitude	-15 dB~15 dB	1 dB	31
Excitation Phase	-180 degree ~ 170 degree	10 degree	36

An ANN with 4 hidden layers was used to predict the temperature rise of the SNM as shown in Figure 2. The input raw data for the ANN consists of 9 input parameters as shown in Table 1. All the categorical values such as human model, IPG position, and IPG side, etc. are preprocessed to numerical values using label encoding [15]. The output of the ANN was the temperature rise. Non-uniform numbers of neurons for each dense layer were used to fit the non-linear relationship between the richer representations of the input data and output temperature rise [9]. The number of the

neurons was decreased gradually to map the high dimensional output from the previous layer to lower-dimensional input in the next layer. Therefore, the final output layer with temperature rise was able to learn the linear relationship from the lower-dimensional space from the output of the last dense layer [16]. The training time of the network was less than 15 seconds and the ANN was implemented by using the TensorFlow framework [17].

The original training set was chosen using an incident electromagnetic field excitation magnitude interval of 5dB and a phase interval of 30 degrees. Thus, the total number of training data used for training was $5 \times 2 \times 2 \times 2 \times 3 \times 2 \times 2 \times 7 \times 12 = 40{,}320$ cases. The rest which was excluded from the training set was used as the test set which has a total number of 495,360 cases.

The test data are used to examine the validity of the ANN by comparing the predicted results with ground truth results. The ANN was optimized by using the Adam stochastic optimization algorithm [18]. Finally, the performance of the ANN was evaluated using the metric of mean absolute error (MAE) and correlation coefficient R^2 [19] between the predicted and ground truth temperature rise.

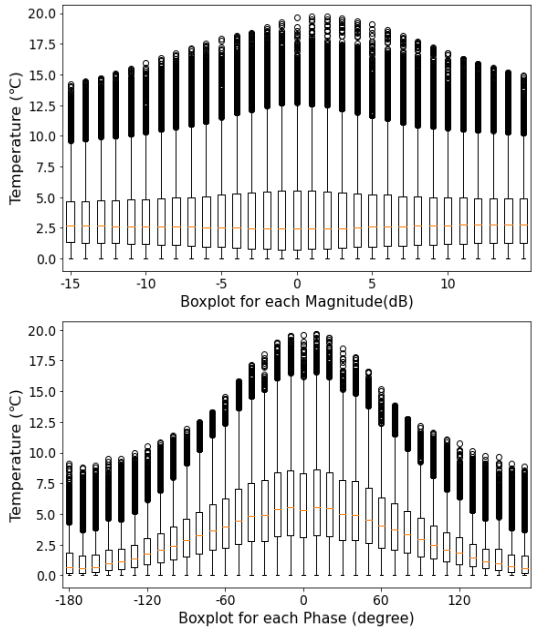

Figure 3. Boxplot simulation results of temperature rise with respect to each excitation magnitude (1dB interval) and each phase (10-degree interval).

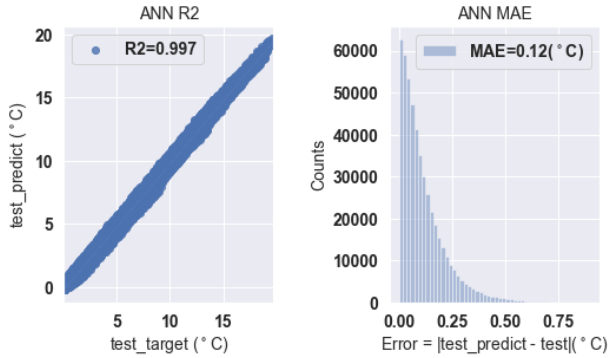

Figure 4. ANN testing performance for all human models.

III. Results

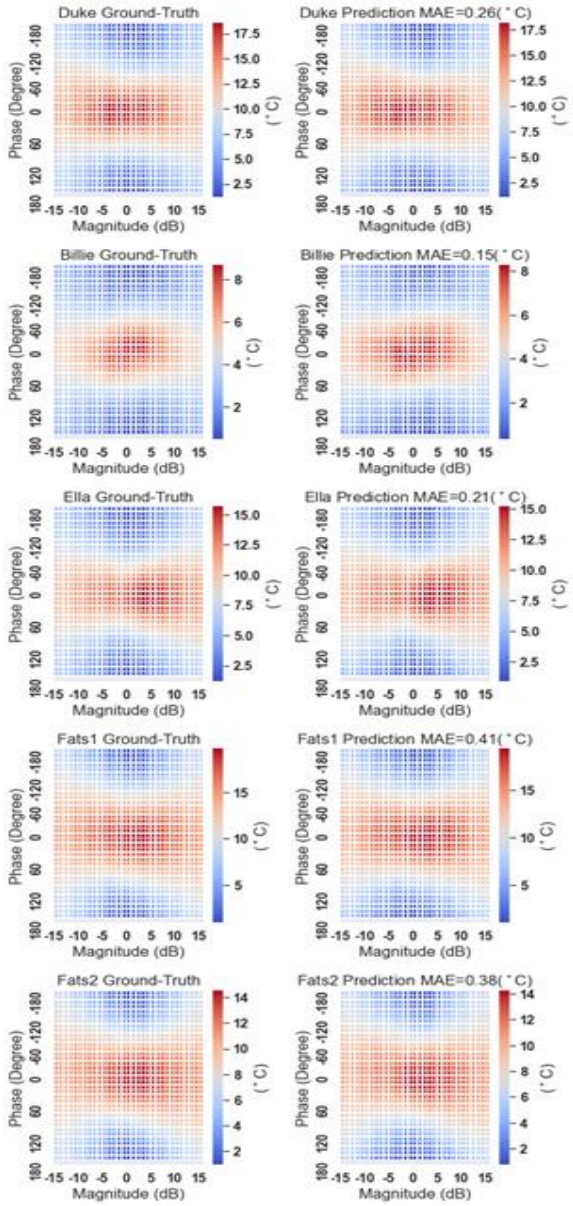

Figure 5. Worst-case temperature prediction using the small exposure sampling space (excitation magnitude interval of 5dB and phase interval of 30 degrees) for five human models: Original ground-truth worst-case temperature (left); Predicted worst-case temperature (right).

The simulation results under the normal operating mode were shown in Figure 3. The magnitude has an interval of the magnitude was 1 dB and in a range from -15 dB to 15 dB. The phase was in a range from -180 degrees to 170 degrees which has an interval of 10 degrees. The maximum temperature rise was as high as $19.70°C$, and the mean temperature rise was $3.49°C$. The variation of the temperature rise was large when different excitation phase was applied. The temperature rise tends to be larger when the phase was small.

The training set (40,320 cases) has an incident electromagnetic field excitation magnitude interval of 5dB and phase interval of 30 degrees to train the ANN and the

rest was used as the test data (495,360 cases) to examine the validity of the network. The correlation coefficient results of the ANN for testing results were shown in Figure 4. The correlation coefficient R^2 between the ground truth temperature and the predicted temperature was larger than 0.99. This indicates that the ANN has learned a non-linear relationship between the input and output. The *MAE* of the ANN was smaller than $0.12°C$ by predicting the test data set. The trained ANN that uses several excitation inputs (excitation magnitude interval of 5dB and phase interval of 30 degrees) can be used to predict the worst-case temperature rise for different human models. As shown in Figure 5, the predicted *MAE* of worst-case temperature for five human models was small compared to the ground truth simulation results. For Duke human model, the predicted *MAE* of worst-case temperature was less than $0.26°C$. Among all five human models, the Billie model has the smallest worst-case temperature prediction *MAE* which was less than $0.15°C$. Fats1 human model has the largest worst-case temperature prediction *MAE* that was close to $0.41°C$. It can be indicated that the worst-case temperature prediction *MAE* of anatomical human models which has a higher body mass index (BMI) tends to be larger due to the heterogenicity of the body tissues that are exposed to the RF field.

TABLE 2. ANN PERFORMANCE USING DIFFERENT TRAINING DATA SIZE.

Training Data (%)	***R2***	***MAE*** **(°C)**
7%	0.997	0.12
5%	0.994	0.16
3%	0.994	0.18
2%	0.991	0.22

The robustness of the ANN models can be demonstrated by studying different size of training data. As shown in the Table 2, the R^2 was larger than and the MAE was less than 0.22 $°C$ with 2% training data. The proposed network predictive models are capable of producing thousands of RF-induced heating predictions within seconds and much faster than the full wave modeling of the devices. Because each device with predefined incident field excitation inside the human model will cost more than 2 hours by the numerical simulation using a NVIDIA C2075 high-performance graphics processing unit (GPU).

IV. CONCLUSION

In this paper, a fast method was proposed to predict the RF-induced heating for the sacral neuromodulation system by using the ANN. To validate this method, the ground truth data were calculated based on the TF method. The RF-induced heating of 535,680 cases was studied to cover all possible shimming conditions by using five different human anatomical body models. For each human model, different combinations of implant positions, excitations, and trajectories were included. This fast method has shown the capability to have good prediction performance from a small exposure sampling space. The testing performance of the ANN has a correlation coefficient higher than 0.99 and the mean absolute error was less than $0.12°C$ using 7% training data. Once the network has been train, the proposed network predictive models are capable of producing thousands of RF-induced heating predictions within seconds. In the future, the ANN architecture needs to be refined and consider a more complex clinical environment.

REFERENCES

[1] *Assessment of the Safety of Magnetic Resonance Imaging for Patients with an Active Implantable Medical Device*, ISO/TS 10974:2012, 2012.

[2] Park, S. M., Kamondetdacha, R., & Nyenhuis, J. A. (2007). Calculation of MRI-induced heating of an implanted medical lead wire with an electric field transfer function. *Journal of Magnetic Resonance Imaging: An Official Journal of the International Society for Magnetic Resonance in Medicine*, *26*(5), 1278-1285.

[3] Feng, S., Qiang, R., Kainz, W., & Chen, J. (2014). A technique to evaluate MRI-induced electric fields at the ends of practical implanted lead. *IEEE Transactions on Microwave Theory and Techniques*, *63*(1), 305-313.

[4] Guo, R., Chen, M., Zheng, J., Yang, R., Chen, J., & Kainz, W. (2017, August). Comparison of in-vivo and in-vitro MRI RF heating for orthopedic implant at 3 tesla. In *2017 IEEE International Symposium on Electromagnetic Compatibility & Signal/Power Integrity (EMCSI)* (pp. 123-128). IEEE.

[5] Ji, X., Zheng, J., & Chen, J. (2017). Numerical evaluation of RF-induced heating for various esophageal stent designs under MRI 1.5 Tesla system. *Electromagnetic Biology and Medicine*, *36*(4), 379-386.

[6] Guo, R., Zheng, J., Wang, Y., Zeng, Q., Wang, Q., Yang, R., ... & Chen, J. (2019). Computational and experimental investigation of RF-induced heating for multiple orthopedic implants. *Magnetic resonance in medicine*, *82*(5), 1848-1858.

[7] Zheng, J., Xia, M., Kainz, W., & Chen, J. (2020). Wire-based sternal closure: MRI-related heating at 1.5 T/64 MHz and 3 T/128 MHz based on simulation and experimental phantom study. *Magnetic Resonance in Medicine*, *83*(3), 1055-1065.

[8] A. S. Childs, S. J. Malik, D. P. O'Regan, and J. V. Hajnal, "Impact of number of channels on RF shimming at 3T," *Magn. Reson. Mater. Physics, Biol. Med.*, vol. 26, no. 4, pp. 401–410, 2013.

[9] Zheng, J., Lan, Q., Zhang, X., Kainz, W., & Chen, J. (2019). Prediction of MRI RF exposure for implantable plate devices using artificial neural network. *IEEE Transactions on Electromagnetic Compatibility*.

[10] Lan, Q., Zheng, J., & Chen, J. (2019, July). Predicting MRI RF Exposure for Complex-shaped Medical Implants Using Artificial Neural Network. In *2019 IEEE International Symposium on Antennas and Propagation and USNC-URSI Radio Science Meeting* (pp. 1861-1862). IEEE.

[11] Lan, Q., Zheng, J., Chen, J., & Zhang, M. (2020, July). Prediction of MRI RF-induced Heating for Passive Implantable Medical Devices Using Convolutional Neural Network. In *2020 IEEE International Symposium on Electromagnetic Compatibility & Signal/Power Integrity (EMCSI)* (pp. 270-275). IEEE.

[12] A Christ, W Kainz, EG Hahn, K Honegger, M Zefferer, E Neufeld, et al., *The virtual family - development of surface-based anatomical models of two adults and two children for dosimetric simulations. Physics in Medicine and Biology*, vol. 55, pp. N23-N28, 2009.

[13] *IT'IS 2010 Virtual Population Project*.

[14] Pennes HH. Analysis of tissue and arterial blood temperatures in the resting human forearm. J Appl Physiol 1948;1:93–122

[15] Hancock, J. T., & Khoshgoftaar, T. M. (2020). Survey on categorical data for neural networks. *Journal of Big Data*, *7*, 1-41.

[16] Karsoliya, S. (2012). Approximating number of hidden layer neurons in multiple hidden layer BPNN architecture. *International Journal of Engineering Trends and Technology*, *3*(6), 714-717.

[17] Brownlee, J. (2016). *Deep learning with Python: develop deep learning models on Theano and TensorFlow using Keras*. Machine Learning Mastery.

[18] Kingma, D. P., & Ba, J. (2014). Adam: A method for stochastic optimization. *arXiv preprint arXiv:1412.6980*.

[19] Helland, I. S. (1987). On the interpretation and use of R2 in regression analysis. *Biometrics*, 61-69.